

Seventh Mississippi State - UAB Conference on Differential Equations and Computational Simulations, *Electronic Journal of Differential Equations*, Conf. 17 (2009), pp. 13–31.
ISSN: 1072-6691. URL: <http://ejde.math.txstate.edu> or <http://ejde.math.unt.edu>
<ftp://ejde.math.txstate.edu>

A COMPUTATIONAL DOMAIN DECOMPOSITION APPROACH FOR SOLVING COUPLED FLOW-STRUCTURE-THERMAL INTERACTION PROBLEMS

EUGENIO AULISA, SANDRO MANSERVISI, PADMANABHAN SESHAIYER

ABSTRACT. Solving complex coupled processes involving fluid-structure-thermal interactions is a challenging problem in computational sciences and engineering. Currently there exist numerous public-domain and commercial codes available in the area of Computational Fluid Dynamics (CFD), Computational Structural Dynamics (CSD) and Computational Thermodynamics (CTD). Different groups specializing in modelling individual process such as CSD, CFD, CTD often come together to solve a complex coupled application. Direct numerical simulation of the non-linear equations for even the most simplified fluid-structure-thermal interaction (FSTI) model depends on the convergence of iterative solvers which in turn rely heavily on the properties of the coupled system. The purpose of this paper is to introduce a flexible multilevel algorithm with finite elements that can be used to study a coupled FSTI. The method relies on decomposing the complex global domain, into several local sub-domains, solving smaller problems over these sub-domains and then gluing back the local solution in an efficient and accurate fashion to yield the global solution. Our numerical results suggest that the proposed solution methodology is robust and reliable.

1. INTRODUCTION

Engineering analysis is constantly evolving with a goal to develop novel techniques to solve coupled processes that arise in multi-physics applications. The efficient solution of a complex coupled system which involves FSTI is still a challenging problem in computational mathematical sciences. The solution of the coupled system provides predictive capability in studying complex nonlinear interactions that arise in several applications. Some examples include a hypersonic flight, where the structural deformation due to the aerodynamics and thermal loads leads to a significant flow field variation or MAVs (Micro Air Vehicles) where geometric changes possibly due to thermal effects may lead to a transient phase in which the structure and the flow field interact in a highly non-linear fashion.

2000 *Mathematics Subject Classification.* 65N30, 65N15.

Key words and phrases. Fluid-structure-thermal interaction; domain decomposition; multigrid solver.

©2009 Texas State University - San Marcos.

Published April 15, 2009.

Supported by grants DMS 0813825 from the National Science Foundation, and ARP 0212-44-C399 from the Texas Higher Education Coordinating Board.

The direct numerical simulation of this highly non-linear system, governing even the most simplified FSTI, depends on the convergence of iterative solvers which in turn relies on the characteristics of the coupled system. Domain decomposition techniques with non-matching grids have become increasingly popular in this regard for obtaining fast and accurate solutions of problems involving coupled processes. The mortar finite element method [1, 2] has been considered to be a viable domain decomposition technique that allows coupling of different subdomains with nonmatching grids and different discretization techniques. The method has been shown to be stable mathematically and has been successfully applied to a variety of engineering applications [3, 4]. The basic idea is to replace the strong continuity condition at the interfaces between the different subdomains by a weaker one to solve the problem in a coupled fashion. In the last few years, mortar finite element methods have also been developed in conjunction with multigrid techniques, [5, 6, 7, 8]. One of the great advantages of the multigrid approach is in the grid generation process wherein the corresponding refinements are already available and no new mesh structures are required. Also, the multigrid method relies only on local relaxation over elements and the solution on different domains can be easily implemented over parallel architectures.

The purpose of this paper is to introduce a flexible multigrid algorithm that can be used to study different physical processes over different subdomains involving non-matching grids with less computational effort. In particular, we develop the method for a model problem that involves Fluid-Structure-Thermal interaction (FSTI). In section 2, the equations of the coupled model are discretized via the finite element discretization. In section 3, the multigrid domain decomposition algorithm to solve the discrete problem is discussed. Finally in section 4 the method is applied to a two-dimensional FSTI application.

2. MODEL AND GOVERNING EQUATIONS

Let the computational domain $\Omega \subset \mathbb{R}^2$ be an open set with boundary Γ . Let the fluid subdomain Ω_f and the solid subdomain Ω_s be two disjoint open sets with boundary Γ_f and Γ_s , respectively and let $\Omega = \Omega_f \cup \Omega_s$.

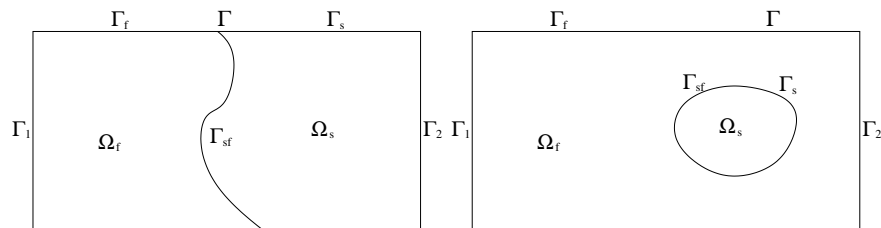


FIGURE 1. Domain $\Omega = \Omega_f \cup \Omega_s$ in two different configurations.

Figure 1 presents illustrations of two sample computational domains. Γ_{sf} is the interior boundary between Ω_f and Ω_s , $\Gamma_f^e = \Gamma \cap \Gamma_f$ is the fluid exterior boundary and $\Gamma_s^e = \Gamma \cap \Gamma_s$ is the solid exterior boundary. For simplicity let us assume that the only boundary which can change in time is the interior boundary Γ_{sf} . In agreement with this assumption both subdomains Ω_f and Ω_s are time dependent

and constrained by

$$\bar{\Omega}_f(t) \cup \bar{\Omega}_s(t) = \bar{\Omega}. \quad (2.1)$$

In the model problem, we employ the unsteady Navier-Stokes equations describing the flow of a fluid in a region Ω_f given by:

$$\begin{aligned} \rho_f \frac{\partial \vec{u}}{\partial t} - \mu_f \Delta \vec{u} + \rho_f (\vec{u} \cdot \nabla) \vec{u} + \nabla p &= \vec{f} \quad \text{in } \Omega_f \times (0, T) \\ \nabla \cdot \vec{u} &= 0 \quad \text{in } \Omega_f \times (0, T) \\ \vec{u} &= \vec{U} \quad \text{on } \Gamma_1 \end{aligned}$$

where ρ_f and μ_f are the density and the viscosity and \vec{f} is the body force. This is coupled with the energy equation given by,

$$\begin{aligned} \rho c_p \frac{\partial T}{\partial t} - k \Delta T + \rho c_p (\vec{u} \cdot \nabla T) &= 0 \quad \text{in } \Omega \times (0, T) \\ T &= \Theta \quad \text{on } \Gamma_2 \end{aligned}$$

that is solved over the whole domain Ω . In the solid region Ω_s the approximate Euler-Bernoulli beam equation is considered. In this approximation plane cross sections perpendicular to the axis of the beam are assumed to remain plane and perpendicular to the axis after deformation [9] and under these hypotheses only a mono-dimensional model is required for the normal transverse deflection field w . We will denote by Λ the beam axis and by (ξ, η) a local reference system oriented with the ξ -axis parallel to Λ .

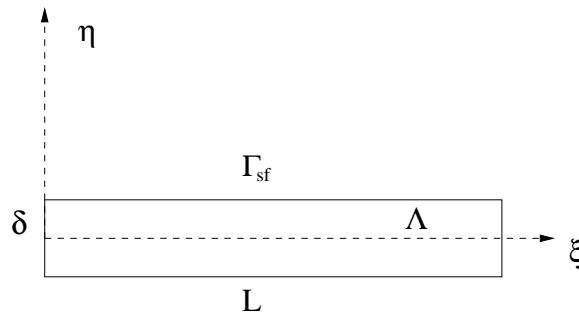


FIGURE 2. Domain notation for the beam domain Ω_s .

As shown in Figure 2, variables δ and L are the thickness and the length of the beam respectively, the interior boundary Γ_{sf} is in $(\xi, \pm\delta/2)$ for $0 \leq \xi \leq L$ and in (L, η) for $-\delta/2 \leq \eta \leq \delta/2$.

In $\Gamma_1 \subset \Gamma_f^e$, Dirichlet boundary conditions are imposed for the velocity field \vec{u} ; Neumann homogenous boundary conditions are considered on the remaining part, $\Gamma_f^e \setminus \Gamma_1$. Similarly, on $\Gamma_2 \subset \Gamma$ Dirichlet boundary conditions are imposed for the temperature T , while Neumann homogenous boundary conditions are considered on $\Gamma \setminus \Gamma_2$. In $\xi = 0$ Dirichlet zero boundary conditions are imposed for the solid displacement w and its derivatives. Conditions of displacement compatibility and force equilibrium along the structure-fluid interface Γ_{sf} are satisfied.

Let $\vec{U} \in \mathbf{H}^{1/2}(\Gamma_1)$ be the prescribed boundary velocity over Γ_1 , satisfying the compatibility condition, and $\Theta \in H^{1/2}(\Gamma_2)$ be the prescribed temperature over Γ_2 .

We are using $H^k(\Omega)$ to denote the space of functions with k generalized derivatives. We set $L^2(\Omega) = H^0(\Omega)$ and note that the derivation of these spaces can be extended to non-integer values k by interpolation. The velocity, the pressure, the temperature and the beam deflection $(\vec{u}, p, T, w) \in \mathbf{H}^1(\Omega_f) \times L^2(\Omega_f) \times H^1(\Omega) \times H^2(\Lambda)$ satisfy the weak variational form of the unsteady fully coupled system given by the Navier-Stokes system over Ω_f ,

$$\begin{aligned} & \langle \rho_f \frac{\partial \vec{u}}{\partial t}, \vec{v}_f \rangle + a_f(\vec{u}, \vec{v}_f) + b_f(\vec{v}_f, p) + c_f(\vec{u}; \vec{u}, \vec{v}_f) \\ & = -\langle \rho_f \vec{g} \beta (T - T_0), \vec{v}_f \rangle \quad \forall \vec{v}_f \in \mathbf{H}^1(\Omega_f), \end{aligned} \quad (2.2)$$

$$b_f(\vec{u}, r_f) = 0 \quad \forall r_f \in L^2(\Omega_f), \quad (2.3)$$

$$\langle \vec{u} - \vec{U}, \vec{s}_f \rangle_{\Gamma_1} = 0 \quad \forall \vec{s}_f \in \mathbf{H}^{-\frac{1}{2}}(\Gamma_1), \quad (2.4)$$

$$\langle \vec{u} - \dot{w} \cdot \hat{n}_{sf}, \vec{s}_{sf} \rangle_{\Gamma_{sf}} = 0 \quad \forall \vec{s}_{sf} \in \mathbf{H}^{-\frac{1}{2}}(\Gamma_{sf}), \quad (2.5)$$

the energy equation over Ω

$$\langle \rho c_p \frac{\partial T}{\partial t}, v \rangle + a(T, v) + c(\vec{u}; T, v) = 0 \quad \forall v \in H^1(\Omega), \quad (2.6)$$

$$\langle T - \Theta, s \rangle_{\Gamma_2} = 0 \quad \forall s \in H^{-\frac{1}{2}}(\Gamma_2), \quad (2.7)$$

and the Euler-Bernoulli beam equation over Ω_s ,

$$\langle \rho_s \delta \ddot{w}, v_s \rangle + a_s(w, v_s) = \langle p(\vec{x}(\xi, -\frac{\delta}{2}), t) - p(\vec{x}(\xi, \frac{\delta}{2}), t), v_s \rangle \quad \forall v_s \in H^2(\Lambda), \quad (2.8)$$

$$w(0, t) = 0, \quad \frac{\partial w(0, t)}{\partial \xi} = 0, \quad \dot{w}(0, t) = 0. \quad (2.9)$$

In (2.2)-(2.3) the continuous bilinear forms are defined as

$$a_f(\vec{u}, \vec{v}) = \int_{\Omega_f} 2\mu_f D(\vec{u}) : D(\vec{v}) d\vec{x} \quad \forall \vec{u}, \vec{v} \in \mathbf{H}^1(\Omega_f), \quad (2.10)$$

$$b_f(\vec{v}, r) = - \int_{\Omega_f} r \nabla \cdot \vec{v} d\vec{x} \quad \forall r \in L^2(\Omega_f), \quad \forall \vec{v} \in \mathbf{H}^1(\Omega_f) \quad (2.11)$$

and the trilinear form as

$$c_f(\vec{w}; \vec{u}, \vec{v}) = \int_{\Omega_f} \rho_f (\vec{w} \cdot \nabla) \vec{u} \cdot \vec{v} d\vec{x} \quad \forall \vec{w}, \vec{u}, \vec{v} \in \mathbf{H}^1(\Omega_f), \quad (2.12)$$

where ρ_f and μ_f are the density and the viscosity of the fluid. The distributed force in Eq. (2.2) is the Boussinesq approximation of the buoyancy force, where \vec{g} is the gravity acceleration, β the volumetric expansion coefficient of the fluid and T_0 a reference temperature. For $T > T_0$ the fluid expands then the density decreases and the buoyancy force points in the direction opposite to the gravity. When $T < T_0$ both the buoyancy force and the gravity point in the same direction. In (2.6) the bilinear form is defined as

$$a(T, v) = \int_{\Omega} k \nabla T \cdot \nabla v d\vec{x} \quad \forall T, v \in H^1(\Omega) \quad (2.13)$$

and the trilinear form

$$c(\vec{u}; T, v) = \int_{\Omega} \rho c_p (\vec{u} \cdot \nabla T) v d\vec{x} \quad \forall \vec{u} \in \mathbf{H}^1(\Omega), \quad T, v \in H^1(\Omega), \quad (2.14)$$

where ρ , c_p , and k are the density, the heat capacity and the heat conductivity, respectively. If the integral is over the subdomain Ω_f , the fluid physical properties ρ_f , c_{p_f} , and k_f are used, otherwise over Ω_s the solid properties ρ_s , c_{p_s} , and k_s are used. Furthermore in the solid region the trilinear form $c(\vec{u}, T, v)$ is identically zero, since the velocity \vec{u} is zero. In (2.8) the bilinear form is defined as

$$a_s(w, v) = \int_{\Lambda} EI \frac{\partial^2 w}{\partial \xi^2} \frac{\partial^2 v}{\partial \xi^2} d\vec{x} \quad \forall w, v \in H^2(\Lambda), \quad (2.15)$$

where EI is the beam stiffness coefficient for unitary deepness. In the right hand side of Eq. (2.8) the load due to the pressure difference between the two sides of the beam is given. (2.8) represents the force equilibrium constraint between the two subdomains Ω_f and Ω_s on the common boundary Γ_{sf} . For details concerning the function spaces, the bilinear and the trilinear forms and their properties, one may consult [9, 10, 11]. Equations (2.4), (2.7) and (2.9) represent the exterior Dirichlet boundary condition for the velocity, the temperature and the displacement, respectively. Eq. (2.5) represents the compatibility constraints between the velocity field \vec{u} and the time derivative of the beam deflection w on Γ_{sf} . The unitary normal \hat{n}_{sf} points in the same direction as the local η -axis. According to Eqs. (2.1) and (2.5), changes in the fluid and solid subdomains Ω_f and Ω_s should be also considered.

2.1. Domain decomposition. Let us now introduce a non-conforming formulation of the problem. Let the domain Ω be partitioned into m non-overlapping sub-domains $\{\Omega^i\}_{i=1}^m$ such that $\partial\Omega^i \cap \partial\Omega^j$ ($i \neq j$) is either empty, a vertex, or a collection of edges of Ω^i and Ω^j . In the latter case, we denote this interface by Γ^{ij} which consists of individual common edges from the domains Ω^i and Ω^j . Let now the fluid domain Ω_f be partitioned into m non-overlapping sub-domains $\{\Omega_f^i\}_{i=1}^m$, where Ω_f^i is given by $\Omega_i \cap \Omega_f$. The fluid partition $\{\Omega_f^i\}_{i=1}^m$ is obtained from the domain partition $\{\Omega^i\}_{i=1}^m$, subtracting the solid region from each subdomain Ω^i , then Ω_f^i is an empty region if Ω^i is a subset of Ω_s . The common boundary between two subregions Ω_f^i and Ω_f^j is denoted by Γ_f^{ij} . The velocity, the pressure, the stress vector, the temperature, the heat flux and the displacement $(\vec{u}^i, p^i, \vec{\tau}^{ij}, T^i, q^{ij}, w) \in \mathbf{H}^1(\Omega_f^i) \times L^2(\Omega_f^i) \times \mathbf{H}^{-1/2}(\Gamma_f^{ij}) \times H^1(\Omega^i) \times H^{-1/2}(\Gamma^{ij}) \times H^2(\Lambda)$ satisfy the following system of equations

$$\begin{aligned} \langle \rho_f \frac{\partial \vec{u}^i}{\partial t}, \vec{v}_f^i \rangle + a_f(\vec{u}^i, \vec{v}_f^i) + b_f(\vec{v}_f^i, p^i) + c_f(\vec{u}^i; \vec{u}^i, \vec{v}_f^i) \\ + \langle \vec{\tau}^{ij}, \vec{v}_f^i \rangle_{\Gamma_f^{ij}} = -\langle \rho_f \vec{g} \beta (T^i - T_0), \vec{v}_f^i \rangle \quad \forall \vec{v}_f^i \in \mathbf{H}^1(\Omega_f^i), \end{aligned} \quad (2.16)$$

$$b_f(\vec{u}^i, r_f^i) = 0 \quad \forall r_f^i \in L^2(\Omega_f^i), \quad (2.17)$$

$$\langle \vec{u}^i - \vec{U}, \vec{s}_f^i \rangle_{\Gamma_1^i} = 0 \quad \forall \vec{s}_f^i \in \mathbf{H}^{-1/2}(\Gamma_1^i), \quad (2.18)$$

$$\langle \vec{u}^i - \vec{u}^j, \vec{s}_f^{ij} \rangle_{\Gamma_f^{ij}} = 0 \quad \forall \vec{s}_f^{ij} \in \mathbf{H}^{-1/2}(\Gamma_f^{ij}), \quad (2.19)$$

$$\langle \vec{u}^i - \dot{w} \cdot \hat{n}_{sf}, \vec{s}_{sf}^i \rangle_{\Gamma_{sf}^i} = 0 \quad \forall \vec{s}_{sf}^i \in \mathbf{H}^{-1/2}(\Gamma_{sf}^i), \quad (2.20)$$

$$\langle \rho c_p \frac{\partial T^i}{\partial t}, v^i \rangle + a(T^i, v^i) + c(\vec{u}^i; T^i, v^i) + \langle \vec{q}^{ij}, \vec{v}^i \rangle_{\Gamma^{ij}} = 0 \quad \forall v^i \in H^1(\Omega^i), \quad (2.21)$$

$$\langle T^i - \Theta, s^i \rangle_{\Gamma_2^i} = 0 \quad \forall s^i \in H^{-1/2}(\Gamma_2^i), \quad (2.22)$$

$$\langle T^i - T^j, \vec{s}^{ij} \rangle_{\Gamma^{ij}} = 0 \quad \forall \vec{s}^{ij} \in H^{-1/2}(\Gamma^{ij}), \quad (2.23)$$

$$\langle \rho_s \delta \ddot{w}, v_s \rangle + a_s(w, v_s) = \langle p(\vec{x}(\xi, -\frac{\delta}{2}), t) - p(\vec{x}(\xi, \frac{\delta}{2}), t), v_s \rangle \quad \forall v_s \in H^2(\Lambda), \quad (2.24)$$

$$w(0, t) = 0, \quad \frac{\partial w(0, t)}{\partial \xi} = 0, \quad \dot{w}(0, t) = 0, \quad (2.25)$$

for $i = 1, 2, \dots, m$ where $\Gamma_1^i = \Gamma_1 \cap \partial\Omega_f^i$, $\Gamma_2^i = \Gamma_2 \cap \partial\Omega^i$, the stress vector $\vec{\tau}^{ij} = -\mu \nabla \vec{u}^i \cdot \hat{n}_f^{ij} + p^i \hat{n}_f^{ij}$ and the heat flux $q^{ij} = -k \nabla T^i \cdot \hat{n}^{ij}$, with \hat{n}_f^{ij} and \hat{n}^{ij} the unitary external vectors normal to the subdomains Ω_f^i and Ω^i , respectively.

Note that in the continuous case, on the boundary Γ_f^{ij} , the velocity vectors, \vec{u}^i and \vec{u}^j are in the same space $\mathbf{H}^{1/2}(\Gamma_f^{ij})$, namely we have $\vec{u}^i = \vec{u}^j$ pointwise. The same remark can be applied to the stress vectors $\vec{\tau}^{ij}$ and $\vec{\tau}^{ji}$, the temperatures T^i and T^j and the heat fluxes q^{ij} and q^{ji} . In the rest of the paper, the variables \vec{u} , p and T , without the label i , should be considered as a collection of all the local variables \vec{u}^i , p^i and T^i , where

$$\begin{aligned} \vec{u}(\vec{x}, t) &= \vec{u}^i(\vec{x}, t) \quad \forall \vec{x} \in \Omega_f^i, \\ p(\vec{x}, t) &= p^i(\vec{x}, t) \quad \forall \vec{x} \in \Omega_f^i, \\ T(\vec{x}, t) &= T^i(\vec{x}, t) \quad \forall \vec{x} \in \Omega^i, \end{aligned}$$

for $i = 1, 2, \dots, m$. It is straightforward to prove that the system (2.16)-(2.25) for the local state variables $(\vec{u}^i, p^i, \vec{\tau}^{ij}, T^i, q^{ij}, w)$, for $i = 1, 2, \dots, m$, implies the system (2.2)-(2.9) for the global state variables $(\vec{u}, p, \vec{\tau}, T, q, w)$.

2.2. ALE formulation and time discretization. In order to account for the changing nature of the fluid and solid subdomains, we wish to define a dynamic mesh for the space discretization. However, to avoid extreme distortion, we choose to move the mesh independently of the fluid velocity in the interior of Ω_f . Such a scheme, called arbitrary Lagrangian-Eulerian (ALE) formulation, is commonly applied when studying fluid-structure interaction [12, 13, 14, 15]. Inside the solid region each point is moving according to the time derivative of the displacement w . The grid velocity \vec{u}_g can be any velocity satisfying the following constraints

$$\vec{u}_g = 0 \quad \text{on } \Gamma, \quad (2.26)$$

$$\vec{u}_g = \vec{u} \quad \text{on } \Gamma_{sf}, \quad (2.27)$$

$$\vec{u}_g(\vec{x}(\xi, \eta), t) = \dot{w}(\xi, t) \hat{n}_{sf} \quad \text{in } \Omega_s. \quad (2.28)$$

If the grid velocity is known as a function of time, the trajectory inside the domain Ω of a generic point of coordinate $\vec{x}(t)$ can be traced by solving the integral equation

$$\vec{x}(t_1) = \vec{x}(t_0) + \int_{t_0}^{t_1} \vec{u}_g(\vec{x}(t'), t') dt'. \quad (2.29)$$

The Lagrangian derivative of the velocity field $\vec{u}(\vec{x}(t), t)$, evaluated along the point trajectory, is given by

$$\begin{aligned} \frac{D \vec{u}(\vec{x}(t), t)}{Dt} &= \frac{\partial \vec{u}}{\partial t} + \frac{\partial \vec{u}}{\partial x_1} \frac{dx_1}{dt} + \frac{\partial \vec{u}}{\partial x_2} \frac{dx_2}{dt} \\ &= \frac{\partial \vec{u}}{\partial t} + \frac{\partial \vec{u}}{\partial x_1} u_{g_1} + \frac{\partial \vec{u}}{\partial x_2} u_{g_2} \\ &= \frac{\partial \vec{u}}{\partial t} + (\vec{u}_g \cdot \nabla) \vec{u}. \end{aligned} \quad (2.30)$$

Then the Eulerian derivative can be written as the difference between the Lagrangian derivative and the corresponding grid velocity advection term

$$\frac{\partial \vec{u}}{\partial t} = \frac{D \vec{u}(\vec{x}(t), t)}{Dt} - (\vec{u}_g \cdot \nabla) \vec{u}. \quad (2.31)$$

In the same way the Eulerian derivative of the temperature T can be expressed as the difference between the Lagrangian derivative and the corresponding grid velocity advection term

$$\frac{\partial T}{\partial t} = \frac{DT(\vec{x}(t), t)}{Dt} - (\vec{u}_g \cdot \nabla) T. \quad (2.32)$$

Using (2.31)-(2.32) in system (2.16)-(2.25), the Navier-Stokes and energy conservation equations become

$$\begin{aligned} \langle \rho_f \frac{D \vec{u}^i(\vec{x}(t), t)}{Dt}, \vec{v}_f^i \rangle + a_f(\vec{u}^i, \vec{v}_f^i) + b_f(\vec{v}_f^i, p^i) + c_f(\vec{u}^i - \vec{u}_g^i; \vec{u}^i, \vec{v}_f^i) + \langle \vec{\tau}^{ij}, \vec{v}_f^i \rangle_{\Gamma_f^{ij}} \\ = -\langle \rho_f \vec{g} \beta(T^i - T_0), \vec{v}_f^i \rangle \end{aligned} \quad (2.33)$$

$$\langle \rho c_p \frac{DT^i(\vec{x}(t), t)}{Dt}, v^i \rangle + a(T^i, v^i) + c(\vec{u}^i - \vec{u}_g^i; T^i, v^i) + \langle \vec{q}^{ij}, \vec{v}_f^i \rangle_{\Gamma^{ij}} = 0.$$

Given the initial velocity field \vec{u}_0 the Lagrangian derivatives can be discretized in time using a simple first order integration method.

The structural equation is discretized in time by a using Newmark integration scheme [9]. In this method the displacement and its time derivative are approximated according to

$$w_{t+1} = w_t + \Delta t \dot{w}_t + \frac{1}{2} \Delta t^2 \ddot{w}_{t+\gamma}, \quad (2.34)$$

$$\dot{w}_{t+1} = \dot{w}_t + \Delta t \ddot{w}_{t+\alpha}, \quad (2.35)$$

where

$$\ddot{w}_{t+\theta} = (1 - \theta) \ddot{w}_t + \theta \ddot{w}_{t+1}, \quad (2.36)$$

and α and γ are parameters that determine the stability and accuracy of the method. We chose $\alpha = \gamma = 0.5$, which is known as the constant-average acceleration method. This technique is stable for each time step Δt and conserves energy for free vibration problem. The use of (2.34)-(2.36) in (2.24) gives the following

approximation

$$\begin{aligned} & \langle \rho_s \delta(a_3 w_{t+1}), v_s \rangle + a_s(w_{t+1}, v_s) - \langle (p_{t+1}(\vec{x}(\xi, -\frac{\delta}{2}), t) - p_{t+1}(\vec{x}(\xi, \frac{\delta}{2}), t), v_s \rangle \\ & = \langle \rho_s \delta(a_3 w_t + a_4 \dot{w}_t + a_5 \ddot{w}_t), v_s \rangle, \\ & a_3 = \frac{2}{\gamma \Delta t^2}, \quad a_4 = \frac{2}{\gamma \Delta t}, \quad a_5 = \frac{1}{\gamma} - 1, \end{aligned} \tag{2.37}$$

where all the terms in the right hand side, w_t , \dot{w}_t and \ddot{w}_t , are evaluated at the previous time step. Note that the calculation of the right hand side requires knowledge of the initial conditions w_0 , \dot{w}_0 and \ddot{w}_0 . In practice, one does not have \ddot{w}_0 . As an approximation, it can be calculated from (2.24)

$$\langle \rho_s \delta \ddot{w}_0, v_s \rangle = \langle p_0(\vec{x}(\xi, -\frac{\delta}{2}), t) - p_0(\vec{x}(\xi, \frac{\delta}{2}), t), v_s \rangle - a_s(w_0, v_s),$$

for given initial displacement w_0 and initial pressure p_0 . At the end of each time step, the new velocity \dot{w}_{t+1} and acceleration \ddot{w}_{t+1} are computed using

$$\begin{aligned} \ddot{w}_{t+1} &= a_3(w_{t+1} - w_s) - a_4 \dot{w}_t - a_5 \ddot{w}_t, \\ \dot{w}_{t+1} &= \dot{w}_t + a_2 \ddot{w}_t + a_1 \ddot{w}_{t+1}, \\ a_1 &= \alpha \Delta t, \quad a_2 = (1 - \alpha) \Delta t. \end{aligned} \tag{2.38}$$

3. SYSTEM DISCRETIZATION

3.1. Multilevel domain decomposition. In this section a multilevel domain decomposition methodology will be described for the whole domain Ω and the corresponding variable T . The same consideration can be directly extended to the fluid domain Ω_f and the corresponding variables \vec{u} and p .

Let us introduce a finite element discretization in each subdomain Ω^i through the mesh parameter h which tends to zero. Let $\{\Omega_h^i\}_{i=1}^m$ be the partition of the discretized domain Ω_h . Now, by starting at the multigrid coarse level $l = 0$, we subdivide each Ω_h^i and consequently Ω_h into triangles or rectangles by families of meshes $\mathcal{T}_h^{i,0}$. Based on a simple element midpoint refinement different multigrid levels can be built to reach the finite element meshes $\mathcal{T}_h^{i,n}$ at the top finest multigrid level $l = n$. At the coarse level, as at the generic multigrid level l , the triangulation over two adjacent subdomains, Ω_h^i and Ω_h^j , obeys the finite element compatibility constraints along the common interfaces Γ_h^{ij} . For details on multigrid levels and their construction one may consult [16, 17, 18].

By using this methodology we have constructed a sequence of meshes for each multigrid level in a standard finite element fashion with compatibility enforced across all the element interfaces built over midpoint refinements. In every subdomain Ω_h^i the energy equations can be solved over a different level mesh, generating a global solution over Ω_h , consisting mesh solutions at different levels over different subdomains. Let $\Omega_h^{i,l}$ be the subdomain i where the solution will be computed at the multigrid level l . It should be noted that the multigrid levels at which the solution is computed over adjacent subdomains, $\Omega_h^{i,l}$ and $\Omega_h^{j,k}$, may be different from each other ($l \neq k$), with no compatibility enforced across the common interface Γ_h^{ij} .

In Figure 3 an example of non-conforming mesh partitioning is given for a square domain Ω_h (Figure 3.a). The square is divided in four subdomains (Figure 3.b) and 3 conforming level meshes are considered ($l = 0, 1, 2$). The coarse mesh (Figure 3.c)

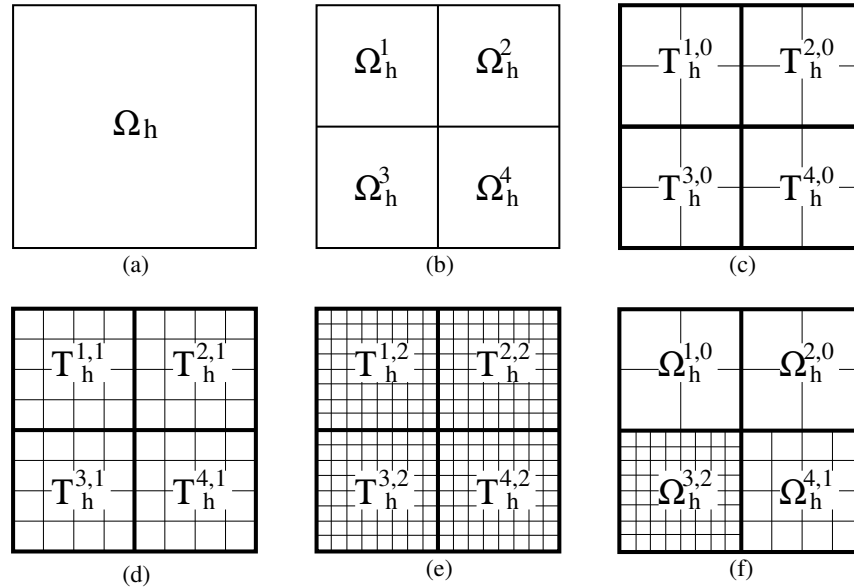


FIGURE 3. Domain (a), domain partitioning (b), conforming coarse level mesh (c), midpoint refinement generation of two finer conforming level meshes (d),(e), non-conforming mesh (f).

is given, while the other two (Figures 3.d-e) are generated by successive midpoint refinements. In Figure 3.f one possible non-conforming mesh configuration is illustrated. Note that in Figure 3.f only across the common boundary $\Gamma_h^{1,2}$ finite element compatibility is obtained since the two subdomain meshes $\Omega_h^{1,0}$ and $\Omega_h^{2,0}$ are chosen at the same level ($l = 0$). On the other three common boundaries, $\Gamma_h^{1,3}$, $\Gamma_h^{2,4}$ and $\Gamma_h^{3,4}$, compatibility is not enforced since different level meshes are considered between two adjacent subdomains. It should be noticed that on the common boundaries the nodes of the coarsest grid are always included in the nodes of the finest one. This is the key point for discretization and resolution of (2.16)-(2.25) and it is always true for different level meshes generated by using midpoint refinements.

Finite element approximation spaces can be generated regularly, as function of the characteristic length h over each multigrid level l resulting in different approximation spaces over the solution meshes $\Omega_h^{i,l}$. In the rest of the paper we denote with labels i, l the solution over the corresponding subdomains, i.e., for the temperature $T^{i,l}$, and with no labels the extended solution over Ω , i.e. T_h for the extended temperature. Note that the temperature $T^{i,l}$ is computed over each $\Omega_h^{i,l}$ at the corresponding level l , but the extended solution T_h on the top level n is defined over all Ω_h in a standard and regular way. There may be parts of the domain where the solution is not computed at the top level but a projection operator \mathcal{I}_l^n from the coarse level l to the top level n can always be used to interpolate the solution over Ω_h . The extended temperature is therefore defined by

$$T_h(\vec{x}, t) = \mathcal{I}_l^n T^{i,l}(\vec{x}, t),$$

for all $\vec{x} \in \Omega_h^i$, $i = 1, 2, \dots, m$. We can easily generalize the notations and evaluate the extended velocity and pressure by using the same operator \mathcal{I}_l^n as

$$\vec{u}_h(\vec{x}, t) = \mathcal{I}_l^n \vec{u}^{i,l}(\vec{x}, t), \quad (3.1)$$

$$p_h(\vec{x}, t) = \mathcal{I}_l^n p^{i,l}(\vec{x}, t), \quad (3.2)$$

for all $\vec{x} \in \Omega_{h_f}^i$, $i = 1, 2, \dots, m$, where $\{\Omega_{h_f}^i\}_{i=1}^m$ is the partition over the discrete subdomains of Ω_{h_f} . These extended functions take the same values over the coarse and the top mesh at those nodes included in both meshes.

3.2. Non-conforming finite element discretization. Let $\mathbf{X}_h^l(\Omega_f) \subset \mathbf{H}^1(\Omega_f)$, $S_h^l(\Omega_f) \subset L^2(\Omega_f)$, $\mathbf{R}_h^l(\Gamma_f) = \mathbf{X}_h^l|_{\Gamma_f} \subset \mathbf{H}^{1/2}(\Gamma_f)$, $X_h^l(\Omega) \subset H^1(\Omega)$ and $R_h^l(\Gamma) = X_h^l|_{\Gamma} \subset H^{1/2}(\Gamma)$ be the approximation spaces. At each level mesh l we chose the families of finite element spaces to satisfy appropriate stability and approximation properties [19, 20] that will allow us building a regular conforming approximation. We indicate with $\mathbf{P}_h^l(\Gamma_f) \subset \mathbf{H}^{-1/2}(\Gamma_f)$ the dual space of $\mathbf{R}_h^l(\Gamma_f)$ and with $P_h^l(\Gamma) \subset H^{-1/2}(\Gamma)$ the dual space of $R_h^l(\Gamma)$. The beam space discretization is obtained by choosing the family of Hermitian elements, $Z_h(\Lambda) \subset H^2(\Lambda)$, for which the interpolation functions are continuous with non-zero derivatives up to order two.

Let J^i be the set of the j -indices of all the neighboring regions Ω^j surrounding the subdomain Ω^i and J_f^i be the set of the j -indices of all the neighboring regions Ω_f^j surrounding the subdomain Ω_f^i . Let $(\vec{u}^{i,l}, p^{i,l}, \vec{\tau}^{ij,l}, T^{i,l}, q^{ij,l}, w)$ be in $\mathbf{X}_h^l(\Omega_f^i) \times S_h^l(\Omega_f^i) \times \mathbf{P}_h^l(\Gamma_f^{ij}) \times X_h^l(\Omega^i) \times P_h^l(\Gamma^{ij}) \times H^2(\Lambda)$ be the velocity, the pressure, the stress vector, the temperature, the heat flux and the beam displacement over the corresponding subdomains. The variable state $(\vec{u}^{i,l}, p^{i,l}, \vec{\tau}^{ij,l}, T^{i,l}, q^{ij,l}, w)$ satisfies the Navier -Stokes discrete system

$$\begin{aligned} & \langle \rho_f \frac{D \vec{u}^{i,l}(\vec{x}_h, t)}{Dt}, \vec{v}_f^{i,l} \rangle + a_f(\vec{u}^{i,l}, \vec{v}_f^{i,l}) + b_f(\vec{v}_f^{i,l}, p^{i,l}) \\ & + c_f(\vec{u}^{i,l} - \vec{u}_g^{i,l}; \vec{u}^{i,l}, \vec{v}_f^{i,l}) + \langle \vec{\tau}^{ij,l}, \vec{v}_f^{i,l} \rangle_{\Gamma_{fh}^{ij}} \end{aligned} \quad (3.3)$$

$$= -\langle \rho_f \vec{g} \beta (T^{i,l} - T_0), \vec{v}_f^{i,l} \rangle \quad \forall \vec{v}_f^{i,l} \in \mathbf{X}_h^l(\Omega_f^i),$$

$$b_f(\vec{u}^{i,l}, r_f^{i,l}) = 0 \quad \forall r_f^{i,l} \in L^2(\Omega_f^i), \quad (3.4)$$

$$\langle \vec{u}^{i,l} - \vec{U}, \vec{s}_f^{i,l} \rangle_{\Gamma_{1h}^i} = 0 \quad \forall \vec{s}_f^{i,l} \in \mathbf{P}_h^l(\Gamma_1^i), \quad (3.5)$$

$$\langle \vec{u}^{i,l} - \vec{u}^{j,k}, \vec{s}_f^{ij,l} \rangle_{\Gamma_{fh}^{ij}} = 0 \quad \forall \vec{s}_f^{ij,l} \in \mathbf{P}_h^l(\Gamma_f^{ij}), \quad (3.6)$$

$$\langle \vec{u}^{i,l} - \dot{w}_h \cdot \hat{n}_{sf}, \vec{s}_{sf}^{i,l} \rangle_{\Gamma_{sfh}^i} = 0 \quad \forall \vec{s}_{sf}^{i,l} \in \mathbf{P}_h^l(\Gamma_{sf}^i), \quad (3.7)$$

over Ω_f^i for all $j \in J_f^i$ and $i = 1, 2, \dots, m$, the energy equation

$$\langle \rho c_p \frac{DT^{i,l}(\vec{x}_h, t)}{Dt}, v^{i,l} \rangle + a(T^{i,l}, v^{i,l}) \quad (3.8)$$

$$+ c(\vec{u}^{i,l} - \vec{u}_g^{i,l}; T^{i,l}, v^{i,l}) + \langle \vec{q}^{ij,l}, \vec{v}_f^{i,l} \rangle_{\Gamma_{fh}^{ij}} = 0 \quad \forall v^{i,l} \in X_h^l(\Omega^i),$$

$$\langle T^{i,l} - \Theta, s^{i,l} \rangle_{\Gamma_{2h}^i} = 0 \quad \forall s^{i,l} \in P_h^l(\Gamma_2^i), \quad (3.9)$$

$$\langle T^{i,l} - T^{j,k}, \vec{s}^{ij,l} \rangle_{\Gamma_{fh}^{ij}} = 0 \quad \forall \vec{s}^{ij,l} \in P_h^l(\Gamma_f^{ij}), \quad (3.10)$$

over Ω^i for all $j \in J_f^i$ and $i = 1, 2, \dots, m$, and the discrete Euler-Bernoulli beam equation

$$\begin{aligned} & \langle \rho_s \delta \ddot{w}_h, v_{s_h} \rangle + a_s(w_h, v_{s_h}) \\ &= \langle p_h(\bar{x}_h(\xi, -\frac{\delta}{2}), t) - p_h(\bar{x}_h(\xi, \frac{\delta}{2}), t), v_{s_h} \rangle \quad v_{s_h} \in Z(\Lambda), \end{aligned} \tag{3.11}$$

$$w_h(0, t) = 0, \quad \frac{\partial w_h(0, t)}{\partial \xi} = 0, \quad \dot{w}_h(0, t) = 0. \tag{3.12}$$

over Λ . On the shared boundaries $\Gamma_{f_h}^{ij}$ the stress vectors, $\bar{\tau}^{ij,l}$ and $\bar{\tau}^{j,i,k}$, belong to the two different spaces \mathbf{P}_h^l and \mathbf{P}_h^k , and their equivalence should be considered in the weak form by

$$\langle \bar{\tau}^{ij,l}, \bar{v}^{i,l} \rangle_{\Gamma_{f_h}^{ij}} = - \langle \bar{\tau}^{j,i,k}, \bar{v}^{i,l} \rangle_{\Gamma_{f_h}^{ij}}. \tag{3.13}$$

Similarly $q^{ij,l}$ and $q^{j,i,k}$ belong to the two different spaces P_h^l and P_h^k , and

$$\langle q^{ij,l}, v^{i,l} \rangle_{\Gamma_h^{ij}} = - \langle q^{j,i,k}, v^{i,l} \rangle_{\Gamma_h^{ij}}. \tag{3.14}$$

Since different level meshes are generated by using midpoint refinement the boundary vector spaces are nested, with $\mathbf{R}_h^l \subseteq \mathbf{R}_h^k$ and $R_h^l \subseteq R_h^k$, assuming $l \leq k$. Then the traces of the test functions $\bar{v}^{i,l}$ and $v^{i,l}$ on the coarsest boundary can be decomposed as a linear combination of traces of test functions $\bar{v}_a^{j,k}$ and $v_a^{j,k}$ on the finest boundary. Under these hypotheses, Eqs. (3.13) and (3.14) become

$$\langle \bar{\tau}^{ij,l}, \bar{v}^{i,l} \rangle_{\Gamma_f^{ij}} = - \langle \bar{\tau}^{j,i,k}, \sum_a w_a \bar{v}_a^{j,k} \rangle_{\Gamma_{f_h}^{ji}} := - \langle \bar{\tau}^{j,i,k}, \mathcal{R}_k^l \bar{v}^{j,k} \rangle_{\Gamma_{f_h}^{ji}}, \tag{3.15}$$

$$\langle q^{ij,l}, v^{i,l} \rangle_{\Gamma_h^{ij}} = - \langle q^{j,i,k}, \sum_a w_a v_a^{j,k} \rangle_{\Gamma_h^{ji}} := - \langle q^{j,i,k}, \mathcal{R}_k^l v^{j,k} \rangle_{\Gamma_h^{ji}}, \tag{3.16}$$

which means that in (3.3) and (3.8) the Lagrange multipliers $\langle \bar{\tau}^{ij,l}, \bar{v}^{i,l} \rangle_{\Gamma_f^{ij}}$ and $\langle q^{ij,l}, v^{i,l} \rangle_{\Gamma_h^{ij}}$ can be always discretized and computed on the finest grid available on the boundary and then restricted over the coarsest one. Eqs. (3.15) and (3.16), define the restriction operator \mathcal{R}_k^l from the finest to the coarsest vector space.

In (3.6) and (3.10) the equalities between $\bar{u}^{i,l}$ and $\bar{u}^{j,k}$ on the boundary $\Gamma_{f_h}^{ij}$, and between $T^{i,l}$ and $T^{j,k}$ on the boundary Γ_h^{ij} , must be considered in their weak form since the velocities and the temperatures belong to the two corresponding different vector spaces $\mathbf{R}_h^l, \mathbf{R}_h^k$ and R_h^l, R_h^k respectively. Assuming $l \leq k$, the spaces are nested with $\mathbf{R}_h^l \subseteq \mathbf{R}_h^k$ and $R_h^l \subseteq R_h^k$. The weak equations may turn into pointwise equations if the velocities or the temperatures belong to the coarsest spaces \mathbf{R}_h^l or R_h^l , respectively.

3.3. Solution strategy. Although the equation system (3.3)-(3.12) is fully coupled, its solution is achieved with an iterative strategy, where the three systems of equations are solved separately and in succession, always using the latest information, until convergence is reached. An iterative multigrid solver is used for both the Navier-Stokes and the energy equation systems since the number of unknowns could be quite large. For the solution of the beam equation a direct LU decomposition is used.

At each iteration, the linearized Navier-Stokes system is assembled, using the latest updated value of the temperature T and the latest updated value of the grid velocity \bar{u}_g in the nonlinear term $c_f(\bar{u} - \bar{u}_g; \bar{u}, \bar{v}_f)$. In the nonlinear term, the

first of the two velocity \vec{u} is considered explicitly. On the boundary Γ_{sf} Dirichlet boundary conditions are imposed according to the latest updated value of the beam displacement time derivative \dot{w} . A V-cycle multigrid algorithm is used to obtain a new update solution for the pressure p and the velocity \vec{u} . Then the energy equation system is assembled, using the previously evaluated velocity and grid velocity in the advection term $c(\vec{u} - \vec{u}_g; T, v)$. A multigrid V-cycle is solved and updated values of the temperature T are found. Finally the beam equation system is built, where the load field is computed using the previous evaluated pressure p . Since the number of the subdomain unknowns is limited an direct LU decomposition solver can be used for computing the new displacement w and its time derivatives. The grid velocity is then computed according to Eqs. (2.26)-(2.28) and the grid nodes are advected along the corresponding characteristic lines. The whole procedure is repeated until convergence is finally reached.

The Navier-Stokes system (3.3)-(3.7) is solved using a fully coupled iterative multigrid solver [21] with a Vanka-type smoother. Multigrid solvers for coupled velocity/pressure system compute simultaneously the solution for both the pressure and the velocity field, and they are known to be one of the best class of solvers for laminar Navier-Stokes equations (see for examples [17, 18]). An iterative coupled solution for the linearized discretized Navier-Stokes system requires the solution of a large number of sparse saddle point problems. In order to optimally solve the equation system (3.3)-(3.7), involving the unknown stress vector $\vec{\tau}^{ij}$, we use the block Gauss-Seidel method, where each block consists of a small number of degrees of freedom (for details see [18, 21, 22, 23, 24]). The characteristic feature of this type of smoother is that in each smoothing step a large number of small linear systems of equations has to be solved. Each block of equations corresponds to all the degrees of freedom which are connected to few elements. For example, for conforming finite elements, the block may consist of all the elements, containing some pressure vertices. Thus, a smoothing step consists of a loop over all the blocks, solving only the equations involving the unknowns inside the elements that are around the considered pressure vertices. The velocity and pressure variables are updated many times in one smoothing step.

The Vanka smoother employed in our multigrid solver involves the solution of a small number of degrees of freedom given by the conforming Taylor-Hood finite element discretization used. For this kind of element the pressure is computed only at the vertices while the velocity field is computed also at the midpoints. Over the internal part of the generic subregion $\Omega_{f_h}^i$, where there are no boundary elements, our Vanka-block consists of an element and all its neighboring elements. We solve for all the degrees of freedom inside the block, with boundary condition taken on the external boundaries.

For example, in Figure 4, our block consists of four vertex points and 12 midpoints to be solved, for a total of 36 unknowns. We have also used different blocks with different performances but we have found this particular block to be very robust and reliable even at high Reynolds numbers. Examples of computations with this kind of solver can be found in [5, 6, 17, 18].

The fact that the solution is searched locally allows us to solve for $\vec{\tau}^{ij}$ only near the common boundary $\Gamma_{f_h}^{ij}$, where different level meshes are coupled, and to solve inside the subdomains by using Vanka smoother. When solving block elements near the common boundary, distinction should be made if the block element is inside

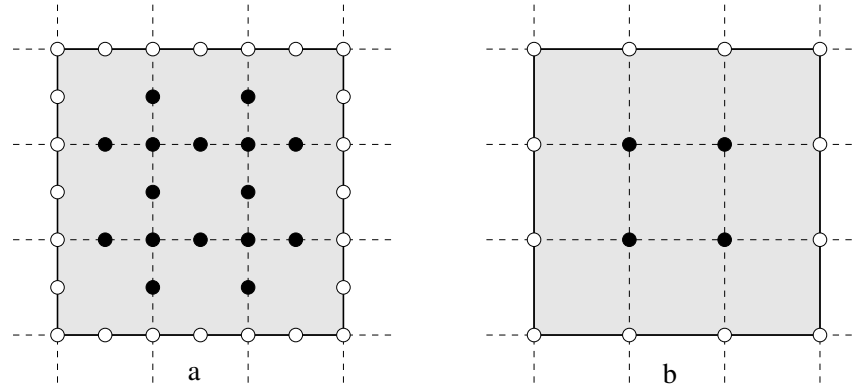


FIGURE 4. Unknowns (black circles) and boundary conditions (white circles) are shown for both the velocity field \vec{u}_h (a) and the pressure p_h (b) for our particular Vanka-block smoother.

the coarse or the fine subregion. Let us consider the two adjacent subdomains $\Omega_{f_h}^{i,l}$ and $\Omega_{f_h}^{j,k}$ with $l \leq k$. We have already seen, that in our particular discretization, where the nodes of the coarsest mesh are included in the finest one, the traces of the two velocities $u^{i,l}$ and $u^{j,k}$ are equal and belong to the coarsest vector spaces \mathbf{R}_h^l . Thus, when solving boundary blocks over the finest subregion $\Omega_{f_h}^{j,k}$, we can use the standard solution technique imposing the trace of the coarsest velocity $u^{i,l}$ as Dirichlet boundary condition for the block equation system. We have also seen that each Lagrange multiplier in the coarsest system can be represented as a linear combination of Lagrange multipliers of the finest system, thus when solving over boundary blocks on the coarsest subregion $\Omega_{f_h}^{i,l}$, the Lagrange multiplier term in (3.3) is replaced with (3.15), where the stress tensor vector $\vec{\tau}^{j,i,k}$ is evaluated over the finest subdomain, by using the pressure, $p^{j,k}$, and velocity field, $\vec{v}^{j,k}$. In this way a constant and reciprocal exchange of information between the two subdomains is ensured.

In order to increase the convergence rate, the considered Vanka-type smoother has been coupled with a standard V-cycle multigrid algorithm. The multigrid does not change the nature of the solver, but allows the information to travel faster among different parts of the domain. A rough global solution is evaluated on the coarsest mesh $l = 0$ and projected on the finer grid $l = 1$, where Vanka-loops are performed improving its details. The updated solution is then projected on the mesh level $l = 2$ and improved. The procedure is repeated until the finest mesh is reached. Solving the equation system in fine meshes improves solution details, but at the same time reduces the communication speed over the domain. However, this does not affect the global convergence rate since a considerable information exchange among different parts of the domain has been already done when solving in coarser mesh levels. The analysis of the convergence of the Vanka type multigrid solvers and the associated invertibility of the discrete system for the Navier-Stokes can be found in [25, 5]. All these considerations can be directly extended to the energy equation solver, where the same element block is considered. For an interior block, as in Figure 4-a, the only unknowns are the values of the temperature at

the vertices and in the midpoints, for a total of 12 variables, while for a boundary block the heat flux $q^{ij,l}$ and $q^{ij,k}$ should be also solved over the common boundary Γ_h^{ij} .

4. NUMERICAL EXPERIMENTS

In this section we test the FSTI non-conforming multilevel formulation and its solution strategy.

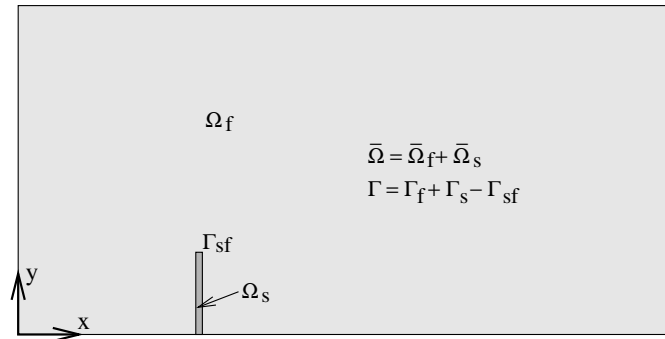


FIGURE 5. Computational domain.

As shown in Figure 5 let the rectangular region $\Omega = [4m] \times [2m]$ be the computational domain with boundary Γ and Ω_f and Ω_s be the fluid and the solid subdomain respectively. The solid region Ω_s consists of a beam, clamped at the point $(1m, 0)$, with length equal to 0.5m and thickness equal to 0.04m. The fluid and the solid boundaries, Γ_f and Γ_s are the contours of the two shaded regions and their intersection is labeled by Γ_{sf} .

On the left side of the domain inflow boundary conditions are imposed for the velocity field $\vec{u} = (u_1, u_2)$ with parabolic profile $u_1 = 0.1y(2-y)m/s$ and $u_2 = 0$. On the right side of the domain outflow boundary conditions are imposed while on the remaining part of the boundary non-slip conditions are set. The temperature is set equal to zero in the inlet region and to $100^\circ C$ on the solid boundary where the beam is clamped. Adiabatic conditions are imposed on the rest of the domain. The initial conditions for both the temperature and the velocity field are zero.

The fluid and the solid properties are chosen in order to produce a large deformation of the beam. This choice implies strong interactions among all the parts of the system and test the reliability of the solver in challenging situations. In the Navier-Stokes system, the fluid density ρ_f , the viscosity μ_f , the volumetric expansion coefficient β and the reference temperature T_0 are equal to $100kg/m^3$, $0.01Kg/m.s$, $0.01K^{-1}$ and $0^\circ C$, respectively. In the temperature equation the solid density ρ_s is $200kg/m^3$, while the heat capacity c_p and the heat conductivity K , are $100J/KgK$ and $10W/mK$ in the fluid region, and $10J/KgK$ and $400W/mK$ in the solid region respectively. The stiffness for unitary length of the beam is equal to $1kgm^2/s^2$.

In all the simulations the same time step $\Delta T = 0.01s$ is used, for a total of 500 time steps (5 seconds). Only the four level meshes, l_0, l_1, l_2 and l_3 , are considered and in Figure 6, the two different level meshes, l_0 and l_3 , are shown.

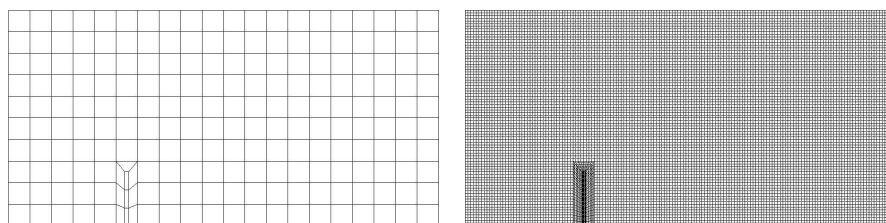


FIGURE 6. The coarse mesh level l_0 (left) and finest level mesh l_3 (right).

The coarse mesh level l_0 has 207 elements, while the mesh level l_3 obtained after three consecutive midpoint refinements has 13248 elements. The one-dimensional mesh on the beam axis follows the same midpoint refinement algorithm used for the two-dimensional computational domain Ω . On the coarse level l_0 three elements are available, while on the fine grid l_3 after 3 refinements, the number of elements becomes 24. Since the number of unknowns is quite small, $(24 + 1) \times 2 = 50$, the solution of the beam equation is always evaluated on the finest mesh using a direct LU decomposition.

The results obtained with our coupled model (case B) are first compared with the results obtained for the same geometry with a rigid beam, $EI = \infty$, and with zero buoyancy force, $\beta = 0$ (case A). All the computations are done at the time $t = 5$ s and over the finest level l_3 .

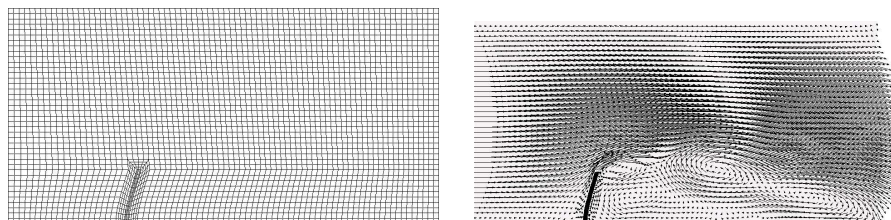


FIGURE 7. Beam bending and grid distortion (left); velocity field map (right).

In Figure 7 on the left, the beam bending and the corresponding grid deformation are displayed, showing the strong influence of the pressure load on the beam shape. Figure 7 on the right shows the velocity field map and clearly indicates that the stationary solution is not reached since new vortices are constantly created and advected towards the outflow region.

In Figure 8 the velocity field (top), the pressure (bottom-left) and the temperature (bottom right) profiles, evaluated over the section $y = 0.5$ for $0 \leq x \leq 4$, are shown for the two cases $EI = \infty$, $\beta = 0$ (case A) and $EI = 1$, $\beta = 0.01$ (case B). The combined effect of the beam deflection and the buoyancy force modify considerably all the profiles, pointing out how sensitive is the interaction among all the parts of the system.

The number of unknowns (velocity field, pressure, temperature and displacement), involved in the computation at the mesh level l_3 is quite large, approximately 94000. However Figure 7 on the right shows that the only part of the system,

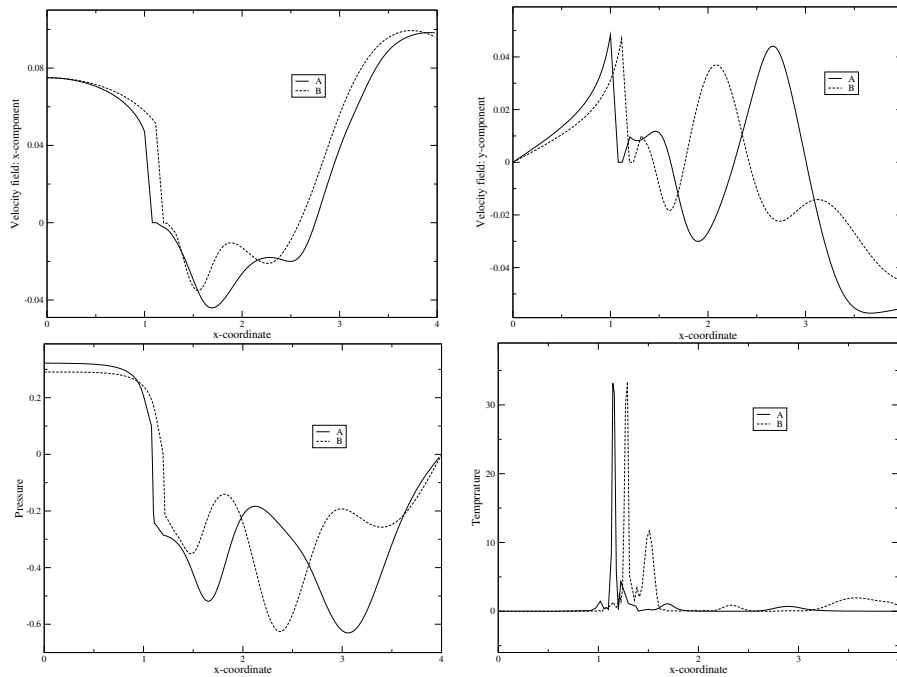


FIGURE 8. Velocity field (top), pressure (bottom-left) and temperature (bottom right) profiles evaluated along the section $y = 0.5$ for $0 \leq x \leq 4$ at the time $t = 5$.

subjected to high vorticity is the region downstream of the beam. In the region upstream of the beam and in the upper part of the domain, the velocity field is almost stationary.

For this reason we remark that more efficient computations can be obtained if the solution is evaluated at the mesh levels l_2 or l_1 in parts of the domain where the mesh level l_3 is not needed. The domain Ω is splitted in three subdomains Ω^1 , Ω^2 , Ω^3 , and three different non-conforming meshes are built. The subdomains and the three different non-conforming partitions are shown in Figure 9.

In the subdomain Ω^3 which is the solid domain Ω_s , the mesh level l_1 is always used. In the first configuration, P_1 (top-right), the mesh levels, l_2 and l_1 , are considered for the subregions Ω^2 and Ω^1 , respectively. The different couplings of level meshes, l_3 - l_2 and l_3 - l_1 are used in the same subregions for the second configuration P_2 (bottom-left), and the third configuration P_3 (bottom-right). The numbers of nodes is greatly reduced for all the three non-conforming configurations. In particular approximately 11000, 39000 and 28000 are the new numbers of unknowns for the new configurations P_1 , P_2 and P_3 , respectively. In Figure 10, the oscillation of the beam extreme point is compared for the three conforming meshes l_0 , l_1 and l_3 , and for the 3 non-conforming meshes P_1 , P_2 and P_3 . The results show clear advantages of the non-conforming discretizations over the conforming ones. Obviously the path obtained with the finest mesh l_3 can be considered the most accurate. The l_2 path is very close to the l_3 in the first second but differences appear as soon as the time increases. The l_1 path is always below the l_3 , showing too much stiffness

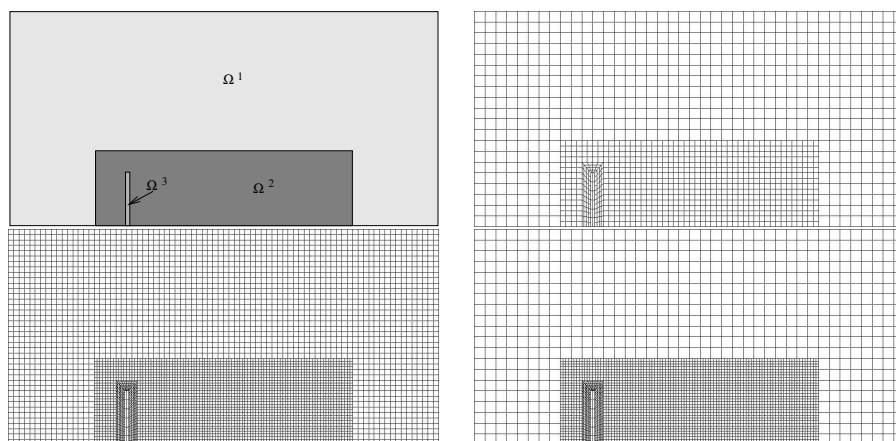


FIGURE 9. Domain decomposition (top-left) and the different configurations P_1 (top-right), P_2 (bottom-left) and P_3 (bottom right).

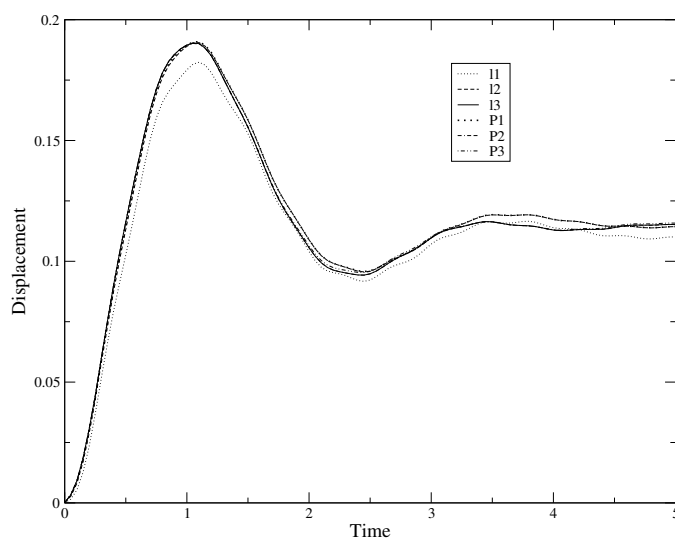


FIGURE 10. Oscillations of the beam extreme point for different conforming and non-conforming meshes.

in the beam response. The beam oscillation obtained with the non-conforming configuration P_1 perfectly overlaps the result obtained with the conforming mesh l_2 , and the result obtained with the configuration P_2 perfectly overlaps the result in l_3 . It is possible to find very small differences between the path in l_3 and the path in P_3 , where there are two mesh levels between the two adjacent regions Ω^1 and Ω^2 . These results clearly indicate how one can use the non-conforming multilevel partitioning to preserve the same accuracy in regions of interest, reducing at the same time the degree of freedom in other parts of the domain. It should be noticed that the comparisons have been tested on a beam displacement oscillation, which is indirectly related to the multilevel domain partitioning. The sensitivity of the

beam's response to the different domain decompositions points out again that the system is fully coupled.

Conclusions. In this paper a multigrid approach applied to the domain decomposition for solving Fluid-Structure-Thermal interaction problems has been presented and tested. Our computational results clearly indicate that the domain decomposition herein used in conjunction with the multigrid method is a robust and reliable technique for solving FSTI systems. The method developed in this paper leads to a fast and flexible algorithm to compute solutions in different domains, over different multigrid levels efficiently. Moreover in [5], we had tested the performance of the computational methodology presented in a parallel environment. The results are very encouraging and the method has prompted us to investigate more open and challenging questions involving coupled problems with fluid-structure-thermal interaction that naturally arise in engineering and science.

REFERENCES

- [1] C. Bernardi, Y. Maday and A. Patera; Domain decomposition by the mortar element method, Asymptotic and numerical methods for partial differential equation with critical parameters. H.K. et al. eds, Reidel, Dordrecht, pp. 269-286, 1993.
- [2] F. Ben Belgacem; The mortar finite element method with Lagrange Multipliers, Numer. Math., vol. 84(2), pp. 173-197, 1999.
- [3] P. Seshaiyer and M. Suri; *hp* submeshing via non-conforming finite element methods, Comput. Meth. Appl. Mech. Eng., vol. 189, pp. 1011-1030, 2000.
- [4] F. Ben Belgacem, L. K. Chilton and P. Seshaiyer; The *hp*-Mortar Finite Element Method for Mixed elasticity and Stokes Problems, Comput. Math. Appl., vol. 46, pp. 35-55, 2003.
- [5] E. Aulisa, S. Manservisi and P. Seshaiyer; A computational multilevel approach for solving 2D Navier-Stokes equations over non-matching grids, to appear in Comput. Meth. Appl. Mech. Eng., vol. 195, pp. 4604-4616, 2006.
- [6] E. Aulisa, S. Manservisi and P. Seshaiyer; A non-conforming computational methodology for modeling coupled problems, Nonlinear Analysis, vol. 6, pp. 1445-1454, 2005.
- [7] D. Braess, W. Dahmen and C. Wieners; A Multigrid Algorithm for the Mortar Finite Element Method, SIAM J. Num. Anal., vol. 37(1), pp. 48-69, 1999.
- [8] J. Gopalakrishnan and J.E. Pasciak; Multigrid for the Mortar Finite Element Method, SIAM J. Num. Anal., vol. 37(3), pp. 1029-1052, 2000.
- [9] J.N. Reddy; An introduction to the finite element method, 2nd Edition, McGraw-Hill, New York, 1993.
- [10] V. Girault and P. Raviart; The Finite Element Method for Navier-Stokes Equations: Theory and Algorithms, Springer, New York, 1986.
- [11] R. Temam; Navier-Stokes equation, North-Holland, Amsterdam, 1979.
- [12] E.W. Swim and P. Seshaiyer; A nonconforming finite element method for fluid-structure interaction problems, Comput. Meth. Appl. Mech. Eng., vol. 195(17-18), pp. 2088-2099, 2006.
- [13] J. Donea, S. Giuliani, J. Halleux; An arbitrary Lagrangian Eulerian finite element method for transient fluid-structure interactions, Comput. Meth. Appl. Mech. Eng., vol. 33, pp. 689-723, 1982.
- [14] C. Grandmont, V. Guimet, Y. Maday; Numerical analysis of some decoupling techniques for the approximation of the unsteady fluid structure interaction, Math. Models Methods Appl. Sci., vol. 11, pp. 1349-1377, 2001.
- [15] T. Hughes, W. Liu, T. Zimmermann; Lagrangian Eulerian finite element formulation for incompressible viscous flows, Comput. Methods Appl. Mech. Engrg., vol. 29, pp. 329-349, 1981.
- [16] J.H. Bramble; Multigrid method, Pitman Research Notes in Math, Longman, London, vol. 294, 1993.
- [17] M. Schafer and S. Turek; The benchmark problem: flow around a cylinder, in Flow simulation with high performance computers II. (E.H. Hirschel ed.), Notes on Numerical Fluid Mechanics, vol. 52, pp. 547, 1996.

- [18] S. Turek; Efficient solvers for incompressible flow problems: an algorithmic and computational approach, Lecture Notes in computational science and engineering, Springer, vol. 6, 1999.
- [19] M. Gunzburger and L.H. Hou; Treating inhomogeneous essential boundary conditions in finite element methods and the calculation of boundary stresses, SIAM J. Num. Anal., vol. 29(2), pp. 390-424, 1992.
- [20] M. Gunzburger, L.H. Hou and T. Svobodny; Analysis and finite element approximations of optimal control problems for the stationary Navier-Stokes equations with Dirichlet control, Math. Model. Numer. Anal., vol. 25, pp. 711-748, 1991.
- [21] S. Vanka; Block-implicit multigrid calculation of two-dimensional recirculation flows, Comput. Meth Appl. Mech. Eng., vol. 59(1), pp. 29-48, 1986.
- [22] V. John; A Comparison of Parallel Solvers for the Incompressible Navier-Stokes Equations, Comput. Visual. Sci., vol. 1(4), pp. 193-200, 1999.
- [23] V. John and L. Tobiska; Numerical Performance of Smoothers in Coupled Multigrid Methods for the Parallel Solution of the Incompressible Navier-Stokes Equations, Int. J. Num. Meth. Fluids, vol. 33, pp. 453-473, 2000.
- [24] M.F. Paisley and N.M. Bhatti; Comparison of multigrid methods for neutral and stably stratified flows over two-dimensional obstacles, J. Comput. Phys., vol. 142, pp. 581-610, 1998.
- [25] S. Manservisi; Numerical Analysis of Vanka-Type Solvers for Steady Stokes and Navier-Stokes Stokes Flows, SIAM J. Numer. Anal., vol. 44, pp. 2025-2056, 2006.

EUGENIO AULISA

MATHEMATICS AND STATISTICS, TEXAS TECH UNIVERSITY, LUBBOCK, TX 79409, USA

E-mail address: eugenio.aulisa@ttu.edu

SANDRO MANSERVISI

DIENCA-LAB. DI MONTECUCCOLINO, VIA DEI COLLI 16, 40136 BOLOGNA, ITALY

E-mail address: sandro.manservisi@mail.ing.unibo.it

PADMANABHAN SESHAIYER

MATHEMATICAL SCIENCES, GEORGE MASON UNIVERSITY, FAIRFAX, VA 22030, USA

E-mail address: pseshaiy@gmu.edu